FREQUENCY DISPERSION OF DIELECTRIC PERMITTIVITY AND ELECTRIC CONDUCTIVITY OF ROCKS VIA TWO-SCALE HOMOGENIZATION OF THE MAXWELL EQUATIONS

V. V. Shelukhin

Lavrentyev Institute of Hydrodynamics
Baker Hughes Incorporated
Lavrentyev Ave. 15, Novosibirsk 630090, Russia

S. A. Terentev

Baker Hughes Incorporated
Kutateladze Ave. 4a, Novosibirsk 630158, Russia

Abstract—We evaluate effective dielectric permittivity and electric conductivity for water-saturated rocks based on a realistic model of a representative cell of the pore space which has periodical structure. We have applied the method of two-scale homogenization of the Maxwell equations, which results in up-scaling coupled equations at the microscale to equations valid at the macroscale. We have analyzed the interfacial Maxwell-Wagner dispersion effect and the Archie law as well.

1. INTRODUCTION

We study behavior of the electromagnetic field in a rock with hetero-geneous microstructure which is described by spatially periodic parameters. We subject such composite materials to the electromagnetic fields generated by currents of varying frequencies. When the period of structure is small compared to a domain of interest, the coefficients in the Maxwell equations oscillate rapidly. These oscillating coefficients are difficult to treat numerically in simulations. Homogenization is a process in which the composite material with microscopic structure is replaced by an equivalent material with macroscopic, homogeneous properties. In this process of homogenization, the rapidly oscillating

Corresponding author: V. V. Shelukhin (shelukhin@hydro.nsc.ru).

coefficients are replaced by new effective constant coefficients. The primary objective of homogenization is to replace a system with periodically varying coefficients by a limiting homogeneous system that facilitates computations.

This way we develop a mixing rule and created a computer code which works well both for DC and AC frequencies. The code was successfully tested by means of comparing effective parameters obtained by the two-scale homogenization presented here and those computed by traditional mixture formulae such as Rayleigh formula or Bruggeman formula. We address the Maxwell-Wagner dispersion effect and Archie's formula. We do not consider here complex geometrical structures and polarization of the double electric layer so our numerical results are applicable to sandstones only.

The concept of two-scale homogenization is a well established tool in the theory of partial differential equations with rapidly oscillating periodic coefficients. The results apply to the equations which aries in porous media, elastic deformation, acoustics, electromagnetism, material sciences, and heat conduction. To justify the approach, mathematical theories have been developed including two-scale expansions, G-convergence, compensated compactness, and two-scale convergence [1, 4, 6, 7, 11–13, 25–27, 30, 35, 37, 39].

A significant amount of research has been done recently on two-scale homogenization of Maxwell's equations. It was proved in many studies that the macroscopic Maxwell equations can be strongly different from the microscopic ones: instantaneous material laws turn into constitutive laws with memory [13, 17–25]. More general case has been considered in [26], with polarization of composite ingredients being not instantaneous but obeying the Debye or Lorenz polarization laws with relaxation. Complexity of the macroscopic constitutive laws is discussed in [27, 28].

The structure of the macroscopic constitutive law can be described in great depth by addressing the time-harmonic Maxwell equations [29–32]. We further develop this research by calculating the effective dielectric constant ε^h and effective electric conductivity σ^h for different values of the angular frequency ω of a source current in the case of several geometric configurations applicable to rock formations. The frequency dispersion of ε^h and σ^h is of importance for the reservoir logging [33]. We prove that the macroequations are different for low and high frequencies when the mixture ingredients are conductive. The result is obtained by the two-scale expansion approach, with $\delta = l/L$ being a small parameter and the ratios l_s/l and l_w/l being taken into account. Here, l is the size of the reference cell of a periodic structure; L is the macroscale size; l_w is the wave length; and l_s is the skin

layer length. Observe that both l_w and l_s depend on ω, the angular frequency of a time-harmonic source current.

The cited publications on the time-harmonic Maxwell equations address homogenization only at low frequencies when the period of the microstructure is small compared to the wave length. Besides, the authors of previous publications do not take into account the skin layer effect while making homogenization. Paper [32] does not involve numerical calculations, and its main result is a mathematical theorem which justifies the macroscopic harmonic Maxwell equations at a fixed low frequency with penetrable boundary conditions. Both the variation of frequency and frequency dispersion of the effective dielectric permittivity are not addressed in [32]. Moreover, the formulas for the effective permittivity and conductivity are restricted to non conductive mixture components; this is why the dispersion effect could not be fixed in this study since the formulas for the effective parameters do not involve the frequency at all.

Numerical evaluation of effective permittivity and effective conductivity on the basis of the two-scale homogenization theory was performed in many publications including [31] for the time-harmonic Maxwell equations (see [26]). The main result of [31] is a successful testing of the numerical algorithm at a fixed low frequency both by comparison of the calculated effective conductivity with those predicted by the Maxwell-Garnett approach [1] and by comparison with an exact electric field related to a specific boundary value problem for the Maxwell equations for the case when inclusions are less conductive than the host medium. As in [31], we also perform numerical evaluation of the effective parameters within the framework of the two-scale homogenization theory but we do not restrict ourselves to the algorithm testing at a fixed frequency. Keeping in mind geophysical applications, we study how effective permittivity and effective conductivity depend on frequency (of a logging tool) for the real rocks when both the less conductive component and the higher conductive component of the mixture form interconnecting structures and when the components conductivity contrast is very high.

The dispersion effect considered in the present paper is due to the Maxwell-Wagner mechanism: free charges concentrate on interphase surfaces to provide continuity of electric currents across such surfaces. This is why resulting polarization of the mixture depends on the source current frequency. When passing to clay-containing rocks one should also take into account bound charges concentrating on the interface surfaces. Such rocks are not considered here.

An important point of the two-scale homogenization method is that the macroscopic material laws are derived by solving

microequations defined on the reference cell. In the case of Maxwell equations, such microscopic equations are reduced to an elliptic system of equations with discontinuous coefficients, which generally can be solved only numerically. To this end we apply a finite element method. But there are some special solid-fluid geometric cell structures when the microequations can be solved analytically. We address a layered and a checkerboard structures to derive formulae for the effective dielectric permittivity and effective electric conductivity at different frequencies. Such a methodical result both serves to test the homogenization approach by comparison with different theories and explains that dispersion of dielectric constant may occur at low frequencies due to complex cell geometry.

Effective electrophysical parameters of electrocomposites were also studied by different physical arguments in [1, 34–37].

The code we developed enables us to report on the statistical Archie's law (1942) which relates effective conductivity to porosity. We discuss limitations of this law and justify its relevance to granular systems evolving geologically from unconsolidated, high-porosity packings toward more consolidated, less porous, materials. The role of geometrical configuration of conducting and non-conducting phases in reservoir rocks was addressed in [2, 38] in the case of low frequencies.

The dispersion effect considered in the present paper is due to the Maxwell-Wagner mechanism: free charges concentrate on interphase surfaces to provide continuity of electric currents across such surfaces. This is why resulting polarization of the mixture depends on the source current frequency. When passing to clay-containing rocks one should also take into account bound charges concentrating on the interface surfaces. Such rocks are not considered here.

2. HOMOGENIZATION OF THE MAXWELL EQUATIONS

2.1. General Periodic Structures

Since water-saturated rocks are notoriously heterogeneous, it is important to have some means of studying the effects of these heterogeneities on the electric fields. To this end, we apply a two-scale homogenization approach. This method requires the microscale length l of the heterogeneous porous medium to be much smaller than the macroscale length L, the latter being of most interest. The method is systematic, leading to Maxwell's equations at the macroscale from an analysis of the microscale variation of electromagnetic parameters (the dielectric permittivity ε, the electric conductivity σ, and the magnetic permeability μ).

Given density of the time-harmonic source current $J_s = e^{-i\omega t}\mathbf{f}(x)$, the incident electric and magnetic fields $E := e^{-i\omega t}\mathbf{E}(x)$, $D := e^{-i\omega t}\mathbf{D}(x)$, $H := e^{-i\omega t}\mathbf{H}(x)$, $B := e^{-i\omega t}\mathbf{B}(x)$, $J := e^{-i\omega t}\mathbf{J}(x)$ solve the Maxwell equations in the SI system of units

$$-i\omega\mathbf{D} = \mathrm{curl}\mathbf{H} - \mathbf{J} - \mathbf{f}, \quad i\omega\mathbf{B} = \mathrm{curl}\mathbf{E}, \tag{1}$$

with the material laws

$$\mathbf{D} = \varepsilon(x)\mathbf{E}, \quad \mathbf{B} = \mu(x)\mathbf{H}, \quad \mathbf{J} = \sigma(x)\mathbf{E}. \tag{2}$$

It is assumed that the mixture components are isotropic media. Periodic rock structure implies that the material functions in (2) are periodic:

$$\varepsilon(x_1+l_1,\, x_2,\, x_3) = \varepsilon(x_1,\, x_2+l_2,\, x_3) = \varepsilon(x_1,\, x_2,\, x_3+l_3) = \varepsilon(x_1,\, x_2,\, x_3),$$

for any x. Similar properties hold for σ and μ. We use the small ratios

$$\frac{l_j}{L} = r_j\delta, \quad \min\{r_1, r_2, r_3\} = 1,$$

where δ is a small dimensionless parameter. The dimensionless parameters r_j characterize deviation of the representative cell of periodicity $Y^\delta = \{0 < x_i < l_i\}$ from a regular cube. Particularly, $r_1 = r_2 = r_3 = 1$ provided all the sizes l_j are equal. We exclude the magnetic fields to obtain the Helmholtz-like equation

$$\mathrm{curl}\left(\mu^{-1}\mathrm{curl}\,\mathbf{E}\right) = \chi^2\mathbf{E} + i\omega\mathbf{f}, \quad \chi^2 = i\omega(\sigma - i\omega\varepsilon). \tag{3}$$

When equation (3) is considered in the entire space, one should set some conditions at infinity. Normally, these are radiation conditions.

Let Y_f^δ and Y_s^δ be the subdomains of Y^δ occupied by fluid and solid respectively, $Y_f^\delta \cup Y_s^\delta = Y^\delta$, and Γ^δ be the interface between the solid and fluid. For simplicity, we consider a composite material with two different components. The coefficients in the Eq. (3) are discontinuous step functions; their restrictions to the representative cell Y^δ are given by the formulae

$$\varepsilon,\, \mu,\, \sigma = \begin{cases} \varepsilon_s,\, \mu_s,\, \sigma_s, & \text{if } x \in Y_s^\delta, \\ \varepsilon_f,\, \mu_f,\, \sigma_f, & \text{if } x \in Y_f^\delta. \end{cases} \tag{4}$$

The boundary conditions at the interfaces Γ^δ is continuity of $\mathbf{n} \times \mathbf{E}$ and $\mathbf{n} \times \mu^{-1}\mathrm{rot}\,\mathbf{E}$, where $\mathbf{n}$ is the unit normal vector to Γ^δ.

As we explain in appendix, the two-scale homogenization approach involves assuming that the field $\mathbf{E}$ can be treated as if it is a function

of two spatial scales x and $y = x/(L\delta)$, with $y \in Y = \{0 < y_j < r_j\}$. The macroscale is x and the microscale is y. Spatial derivatives of $\mathbf{E}$ can then be usefully written as

$$\text{curl}\mathbf{E}(x,\, x/(\delta L)) = \left\{ \text{curl}_x\mathbf{E}(x,\, y) + \frac{1}{\delta L}\text{curl}_y\,\mathbf{E}(x,\, y) \right\}|_{y=x/(\delta L)}. \quad (5)$$

Thus, the scale separation can be explicitly accounted for in such a derivative equation. Furthermore, the field $\mathbf{E}$ can also be treated as a function of δ, so that an asymptotic expansion of the form

$$\mathbf{E}(x,\, y,\, \delta) = \mathbf{E}^0(x,\, y) + \delta\mathbf{E}^1(x,\, y) + o(\delta) \quad (6)$$

may be written. Combining (5) and (6) we arrive at

$$\text{curl}\mathbf{E} = \frac{1}{\delta L}\text{curl}_y\,\mathbf{E}^0(x,\, y) + \text{curl}_x\,\mathbf{E}^0(x,\, y) + \frac{1}{L}\text{curl}_y\,\mathbf{E}^1(x,\, y) + O(\delta),$$

where $y = x/\delta L$, a result which gets used repeatedly in the subsequent analysis. This approach requires a great deal of mathematical insight. All the proofs are given in appendix; here we reproduce final results only. Notice that all the calculations in Appendix are performed in the Gauss system of units with the aim to correctly take into account both the wave length l_w and skin layer length l_s while dealing with the expansion series (6). Here and in the main body of the paper we use the SI system keeping in mind presentation of our numerical calculations and comparison with results published elsewhere.

The incident electric field $\mathbf{E}(x)$ is well-approximated by the macro-field $\tilde{\mathbf{E}}(x)$:

$$\mathbf{E}(x) = \tilde{\mathbf{E}}(x) + \tilde{E}_j(x)\nabla_y w_\varepsilon^j(y) + O(\delta), \quad \text{where} \quad y_j = \frac{r_j x_j}{l_j}. \quad (7)$$

Here, $w_\varepsilon^j(y)$ are dimensionless periodic micro-potentials which solve the following boundary-value problems in the cell Y:

$$\frac{\partial}{\partial y_p}\left\{ (\sigma(y) - i\omega\varepsilon(y))\frac{\partial}{\partial y_p}\left(y_j + w_\varepsilon^j(y) \right) \right\} = 0, \quad \int\limits_Y w_\varepsilon^j(y)dy = 0. \quad (8)$$

The present method produces definite formulae for the effective

matrices ε^h, σ^h, and μ^h with the help of the micro-potentials:

$$\varepsilon_{pj}^h = \frac{1}{|Y|} \int_Y \varepsilon(y) \frac{\partial}{\partial y_p} \left(y_j + w_\varepsilon^j(y) \right) dy, \quad |Y| = r_1 r_2 r_3, \qquad (9)$$

$$\sigma_{pj}^h = \frac{1}{|Y|} \int_Y \sigma(y) \frac{\partial}{\partial y_p} \left(y_j + w_\varepsilon^j(y) \right) dy, \qquad (10)$$

$$\mu_{pj}^h = \frac{1}{|Y|} \int_Y \mu(y) \frac{\partial}{\partial y_p} \left(y_j + w_\mu^j(y) \right) dy. \qquad (11)$$

Here, $w_\mu^j(y)$ are dimensionless periodic micro-potentials which are solutions to the following boundary-value problems in the cell Y:

$$\frac{\partial}{\partial y_p} \left\{ \mu(y) \frac{\partial}{\partial y_p} \left(y_j + w_\mu^j(y) \right) \right\} = 0, \quad \int_Y w_\mu^j(y) dy = 0. \qquad (12)$$

As proved in [13], it follows from (8) and (12) that the matrices ε_{pj}^h, σ_{pj}^h, and μ_{pj}^h are symmetric. The micro-potentials w_ε^j are holomorphic functions of frequency; therefore the Kramers-Kronig relations [39] are fulfilled for the real and imaginary parts of the permittivity function $\varepsilon_{pj}^h(\omega)$.

We prove in appendix that, whereas formulae (9)–(11) are valid over wide ranges of frequency, the macro-equations for the field $\tilde{\mathbf{E}}(x)$ are different for low and high frequencies. The low-frequency macro-equation is

$$\text{curl} \left\{ \left(\mu^h \right)^{-1} \cdot \text{curl} \tilde{\mathbf{E}} \right\} - (\chi^2)^h \cdot \tilde{\mathbf{E}} = i\omega \mathbf{f}, \qquad (13)$$

where

$$\left(\chi^2 \right)_{pj}^h = i\omega \left(\sigma_{pj}^h - i\omega \varepsilon_{pj}^h \right).$$

For high frequencies, the macro-field $\tilde{\mathbf{E}}(x)$ is the solution to the equation

$$-(\chi^2)^h \cdot \tilde{\mathbf{E}} = i\omega \mathbf{f}. \qquad (14)$$

2.2. Layered Structure

Let us test the method on a material with the representative cell composed of two layers (Fig. 1(a)):

$$\varepsilon(y), \, \mu(y), \, \sigma(y) = \begin{cases} \varepsilon_f, \, \mu_f, \, \sigma_f, & \text{if } 0 < y_3 < \Phi_f r_3, \\ \varepsilon_s, \, \mu_s, \, \sigma_s, & \text{if } \Phi_f r_3 < y_3 < r_3, \end{cases} \qquad (15)$$
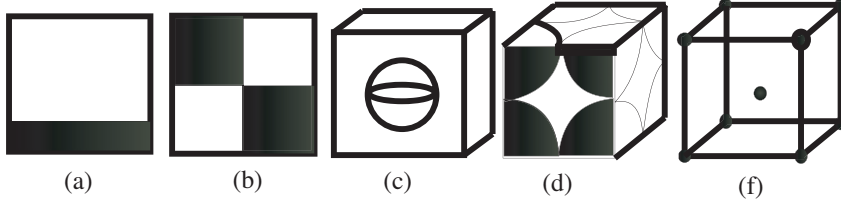
Figure 1. Cell geometry structures: (a) layer (intersection with the plane $y_2 = $ const), (b) checkerboard (intersection with the plane $y_3 = $ const), (c) sphere, (d) Q_8^r-cell with $r = 0.5$, (f) Q_9^r-cell (only sphere centers).

where $0 < \Phi_f < 1$. The cell-problems (8) can be solved analytically. Particularly, one can verify that $w_\varepsilon^1(y) = w_\varepsilon^2(y) = 0$. Hence, $\varepsilon_{pj}^h = 0$ and $\sigma_{pj}^h = 0$ provided $p \neq j$, and

$$\varepsilon_{11}^h = \varepsilon_{22}^h = \Phi_f \varepsilon_f + \Phi_s \varepsilon_s, \quad \sigma_{11}^h = \sigma_{22}^h = \Phi_f \sigma_f + \Phi_s \sigma_s,$$

where Φ_f is the porosity and $\Phi_s \equiv 1 - \Phi_f$. Eq. (8) for $w_\varepsilon^3(y)$ becomes

$$\chi^2(y)\frac{d}{dy_3}\left(y_3 + w_\varepsilon^3\right) = b_0 = \text{const}, \quad \int_0^{r_3} w_\varepsilon^3 dy_3 = 0. \qquad (16)$$

We arrive at $1/b_0 = \Phi_f/\chi_f^2 + \Phi_s/\chi_s^2$. Hence,

$$\varepsilon_{33}^h = \frac{i\omega\varepsilon_f\varepsilon_s - (\Phi_f\varepsilon_f\sigma_s + \Phi_s\varepsilon_s\sigma_f)}{i\omega\left(\Phi_f\varepsilon_s + \Phi_s\varepsilon_f\right) - (\Phi_f\sigma_s + \Phi_s\sigma_f)}, \qquad (17)$$

$$\sigma_{33}^h = \frac{i\omega\left(\Phi_f\varepsilon_s\sigma_f + \Phi_s\varepsilon_f\sigma_s\right) - \sigma_f\sigma_s}{i\omega\left(\Phi_f\varepsilon_s + \Phi_s\varepsilon_f\right) - (\Phi_f\sigma_s + \Phi_s\sigma_f)}. \qquad (18)$$

It should be noted that these formulae coincide with the Maxwell-Wagner laws for the circuit of two layers [40, 41].

We calculate

$$\frac{\varepsilon_{33}^h(\omega) - \varepsilon_{33}^h(\infty)}{\varepsilon_{33}^h(0) - \varepsilon_{33}^h(\infty)} = \frac{1}{1 - i\tau_{33}^h\omega}, \quad \tau_{33}^h \equiv \frac{\Phi_f\varepsilon_s + \Phi_s\varepsilon_f}{\Phi_f\sigma_s + \Phi_s\sigma_f}. \qquad (19)$$

It implies that the homogenized medium obeys a Debye polarization law [42] (in x_3-direction)

$$D = E + P, \quad P = P_1 + P_2, \quad P_1 = \chi_1 E, \quad \frac{d}{dt}P_2 = \frac{\chi_2 E - P_2}{\tau},$$

with relaxation time $\tau = \tau_{33}^h$ and

$$\chi_1 = \varepsilon_{33}^h(\infty) - 1, \quad \chi_2 = \varepsilon_{33}^h(0) - \varepsilon_{33}^h(\infty).$$

Thus, whereas polarization of both the ingredients is instantaneous ($P = \chi_1 E$, with $\chi_1 = \varepsilon_s - 1$ for the solid component and $\chi_1 = \varepsilon_f - 1$ for the fluid component), polarization of the homogenized media (in x_3-direction) consists of the instantaneous part P_1 and relaxation part P_2.

We analyzed dispersion curves by switching to the effective parameters

$$\sigma^e = \mathrm{Re}(\sigma_{33}^h)^*, \qquad \varepsilon^e = -\mathrm{Im}(\sigma_{33}^h)^*/\omega,$$
$$(\sigma^h)^* \equiv \sigma^h - i\omega\varepsilon^h, \quad \sigma_{s,f}^* \equiv \sigma_{s,f} - i\omega\varepsilon_{s,f}.$$

We have

$$\sigma^e(\omega) = \frac{a_\sigma + d_\sigma\omega^2}{c + b\omega^2}, \quad \varepsilon^e(\omega) = \frac{a_\varepsilon + d_\varepsilon\omega^2}{c + b\omega^2}, \tag{20}$$

where

$$
\begin{aligned}
a_\sigma &= \sigma_f\sigma_s(\Phi_f\sigma_s + \Phi_s\sigma_f), & d_\sigma &= \varepsilon_s\varepsilon_s\sigma_f\Phi_f + \varepsilon_f\varepsilon_f\sigma_s\Phi_s, \\
a_\varepsilon &= \sigma_f\sigma_f\varepsilon_s\Phi_s + \sigma_s\sigma_s\varepsilon_f\Phi_f, & d_\varepsilon &= \varepsilon_f\varepsilon_s(\Phi_f\varepsilon_s + \Phi_s\varepsilon_f), \\
b &= (\Phi_f\varepsilon_s + \Phi_s\varepsilon_f)^2, & c &= (\Phi_f\sigma_s + \Phi_s\sigma_f)^2.
\end{aligned}
$$

Because of the formulae

$$
\begin{aligned}
\frac{d}{d\omega}\sigma^e &= \frac{A_\sigma\omega}{(c + b\omega^2)^2}, & \frac{d}{d\omega}\varepsilon_e &= \frac{A_\varepsilon\omega}{(c + b\omega^2)^2}, \\
\frac{d^2}{d\omega^2}\sigma^e &= \frac{A_\sigma(c - 3b\omega^2)}{(c + b\omega^2)^3}, & \frac{d^2}{d\omega^2}\varepsilon_e &= \frac{A_\varepsilon(c - 3b\omega^2)}{(c + b\omega^2)^3},
\end{aligned}
$$

where $A_\sigma = 2(d_\sigma c - a_\sigma b) > 0$, $A_\varepsilon = 2(d_\varepsilon c - a_\varepsilon b) < 0$, the function $\sigma^e(\omega)$ is increasing (Fig. 2) and $\varepsilon^e(\omega)$ is decreasing as $\omega \to \infty$ (Fig. 3). There is a unique Maxwell-Wagner angular frequency ω_{mw}, $\omega_{mw}^2 = c/(3b)$, a center of dispersion, such that the second derivative of both functions with respect to ω vanishes at $\omega = \omega_{mw}$, and the maximum of gradient both of $\sigma_e(\omega)$ and $\varepsilon^e(\omega)$ reaches the dispersion center ω_{mw}. If σ_s is small enough to where $\sigma_s\varepsilon_f < \sigma_f\varepsilon_s$, then the dispersion center $\omega_{mw}(\Phi_f)$ becomes decreasing and drops to values between $\sigma_s/\left(\sqrt{3}\varepsilon_s\right)$ and $\sigma_f/\left(\sqrt{3}\varepsilon_f\right)$.

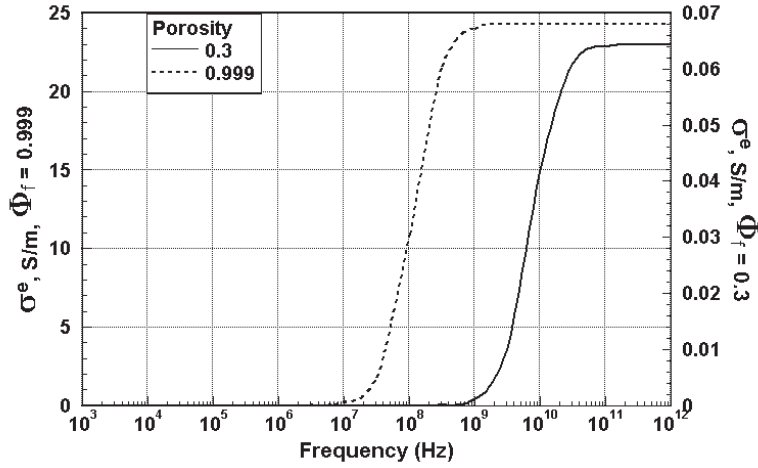**Figure 2.** Dispersion of effective conductivity for the layered structure as in Fig. 1(a) when $\sigma_s = 10^{-12}\,(\text{S/m})$, $\sigma_f = 25\,(\text{S/m})$, $\varepsilon_s/\varepsilon_0 = 4$, $\varepsilon_f/\varepsilon_0 = 60$.

2.3. Checkerboard Structure

There is one more geometrical structure where the effective parameters can be calculated analytically on the basis of Eq. (8). Let the intersection of the representative cell Y with the plane $y_3 = \text{const}$ be like in Fig. 1(b). When both of the components are non-conductors, it can be proved as in [5] that

$$\varepsilon_{11}^h = \varepsilon_{22}^h = \sqrt{\varepsilon_f \varepsilon_s}, \quad \varepsilon_{33}^h = (\varepsilon_f + \varepsilon_s)/2, \quad \varepsilon_{pj}^h = 0 \quad \text{if} \quad p \neq j.$$

These formulae were derived via different arguments in [43]. This square root law is also true for AC frequencies: $(\sigma_{jj}^h)^* = \sqrt{\sigma_f^* \sigma_s^*}$, $j = 1, 2$.

3. DISPERSION CURVES

We solve the cell problems by the finite elements method. The code we developed was tested successfully by solving the cell problems for the layered and checkerboard periodical structures. In Fig. 3 there is a plot of the effective dielectric permittivity dispersion function $\varepsilon^e(\omega)$ for a layered medium and two different values of porosity Φ_f. One can observe that the values of ε^e for low frequencies can be many times
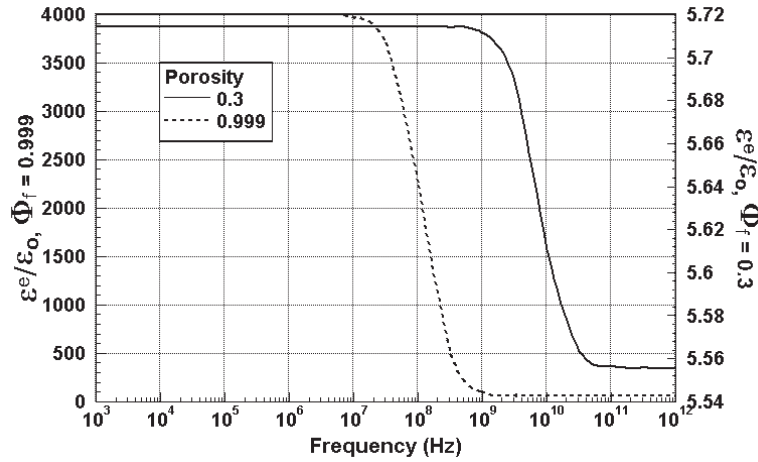
Figure 3. Dispersion of relative effective dielectric permittivity for the layered structure as in Fig. 1(a). The component data are those in Fig. 2.

greater than the component data ε_s and ε_f. This effect is due to high capacity of thin weakly conductive layers and a phase shift of the conduction current. On the other hand, homogenized permittivity ε^h does not differ significantly from the component data ε_s and ε_f for DC frequencies (Fig. 4). The dielectric constant may show dispersive behavior at low frequencies when solid layers are thin. This suggests that the Maxwell-Wagner dispersive behavior at low frequencies may occur for media with complex geometrical structure as well. It should be noted that a theory was also developed in [44] to explain why high values of the effective permittivity ε^e for low frequencies occur in rocks with high porosity, composed of thin plate solid grains. But it is unclear if this explanation is adequate as far as dispersion in clays is concerned, because such rocks are characterized by low porosity.

There is a number of outstanding mixing laws for electrocomposites [1]. We perform comparison with the formula

$$
\frac{\sigma^*}{\sigma_f^*} = 1 - 3\Phi_s \left[\frac{2+\Delta}{1-\Delta} + \Phi_s - \frac{1.306\Phi_s^{10/3}}{\frac{4/3+\Delta}{1-\Delta} + 0.4072\Phi_s^{7/3}} \right.
$$
$$
\left. - \frac{2.218 \times 10^{-2}(1-\Delta)\Phi_s^{14/3}}{6/5+\Delta} \right]^{-1}, \quad \Delta = \sigma_s^*/\sigma_f^*, \qquad (21)
$$

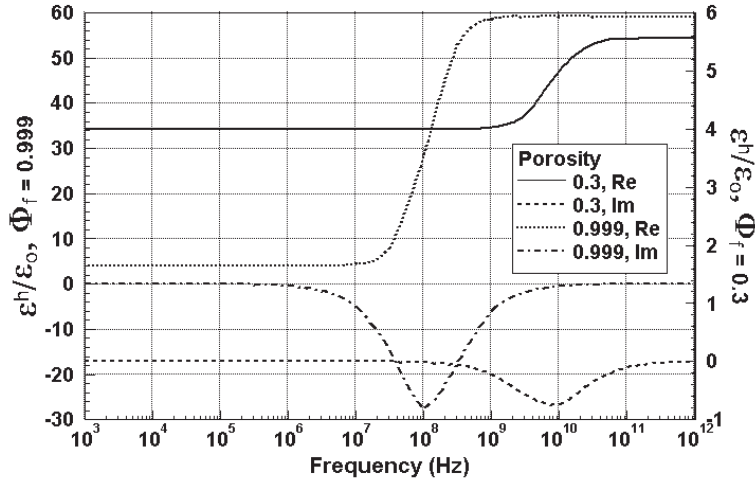which is an extension of the Zuzovsky-Brenner formula [45] for AC

Figure 4. Real and imaginary parts of the homogenized relative dielectric permittivity versus frequency for the layered structure as in Fig. 1(a) for two values of porosity. The component data are those in Fig. 2.

frequencies, derived by the Bruggeman approach. The law (21) is the result of calculations for the effective conductivity of a simple cubic array of spheres (with the data σ_s and ε_s) embedded in a matrix (with the data σ_f and ε_f) versus volume fraction of spheres Φ_s. The plots in Fig. 5 and Fig. 6 calculated for DC frequencies show that the two-scale homogenization rule, derived for the case when Y_s is a sphere (Fig. 1(c)), agrees well with the rule (21) up to Φ_s close to 0.5. The homogenization results begin to diverge from the mixing formula (21) near the point $\Phi_s = 0.5$ due to limitations of the latter.

Next, we consider two more periodical structures. The first, termed Q_8^r, is formed of eight solid spheres of the same radius r centered at the unit cube vertices. Its configuration is given in Fig. 1(d). (Clearly, configurations in Fig. 1(c) and Fig. 1(d) are geometrically identical if the spheres do not intersect each other.) To take into account the formation process of sedimentation rocks, we perform calculations for various values of r, from $r = 0.5$, when a sphere touches neighboring spheres (and when the corresponding $\Phi_{f,\max}$ is approximately equal to 0.4764), to $r_p = \sqrt{2}/2$ (with the corresponding percolation value of Φ_f equal to $\Phi_p \simeq 0.0349$), when the pore space loses connectivity. The grains are allowed to swell equally in all directions to be interpenetrable until the desired volume fraction Φ_s
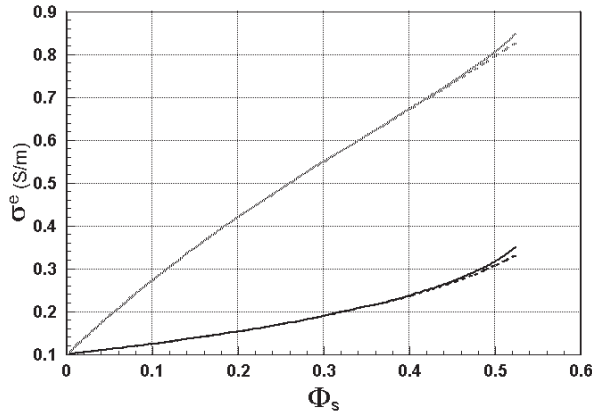
Figure 5. Effective conductivity at two different frequencies versus volume fraction of the sphere inclusions as in Fig. 1(c). The solid curves are calculated by the homogenization approach; the dotted curves are given by the mixing rule like (21). Two upper curves correspond to 10^{11} (Hz); two curves below correspond to 10^3 (Hz). The component data are $\sigma_s = 1$ (S/m), $\sigma_f = 0.1$ (S/m), $\varepsilon_s/\varepsilon_0 = 5$, $\varepsilon_f/\varepsilon_0 = 50$, $\varepsilon_0 = 8.85 \times 10^{-12}$.
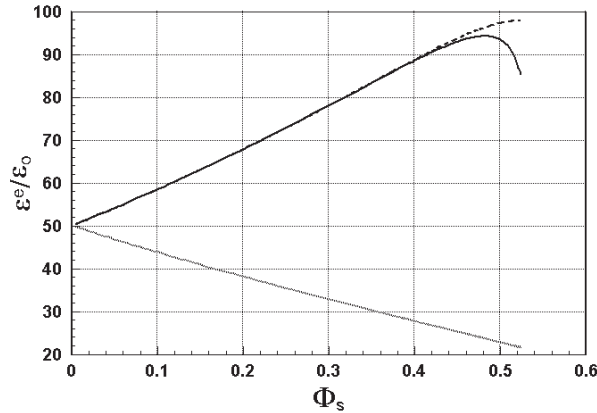

Figure 6. Reduced effective dielectric permittivity at two different frequencies versus volume fraction of the sphere inclusions as in Fig. 1(c). The solid curves are calculated by the homogenization approach; the dotted curves are yielded by a mixing rule like (21). Two upper curves correspond to 10^3 (Hz); two curves below are practically identical and correspond to 10^{11} (Hz). The component data are $\sigma_s = 1(S/m)$, $\sigma_f = 0.1(S/m)$, $\varepsilon_s/\varepsilon_0 = 5$, $\varepsilon_f/\varepsilon_0 = 50$, $\varepsilon_0 = 8.85 \times 10^{-12}$.

is attained. The homogenized medium is isotropic, and the dispersion curves are plotted in Fig. 7 and Fig. 8. To calculate $\Phi_{f,\max}$ and Φ_p one can use the following simple diagenesis law [38]

$$\Phi(r) = 1 - \frac{\pi}{6} - \frac{\pi}{2}\left(\frac{r}{2}-1\right) + \frac{\pi}{4}\left(\frac{r}{2}-1\right)^2 + \frac{\pi}{3}\left(\frac{r}{2}-1\right)^3,$$

which describes how porosity depends on increasing vertex sphere radius. Diagenesis is the process by which granular systems evolve geologically from unconsolidated, high-porosity packings toward more consolidated, less porous, materials. This model retains essential features of many granular porous systems: (1) the pore spaces and grains form interconnecting channels, (2) grains are of comparable size, and (3) the grains are joined at contacts that extend over a finite area.

To permit higher tortuosity, we consider the Q_9^r-cell which is the Q_8^r-cell with one more solid sphere of radius r in the center of the cube (Fig. 1(f)). The grains grow equally in all directions. Radius r varies from $\sqrt{3}/4$, when the center sphere touches the vertex spheres (and when the corresponding $\Phi_{f,\max}$ is approximately equal to 0.3198), to some value $r_p = 3/\sqrt{32} \simeq 0.5303$ (with the corresponding percolation value of Φ_f equal to $\Phi_p \simeq 0.0055$), when pore fluid becomes isolated. The homogenized medium is isotropic, and the dispersion curve does not differ significantly from the Q_8^r-cell case.

We comment on applications. In typical sandstone rocks, the pore size is such that the microscale length l is close to $5 \cdot 10^{-2}$ m, and the
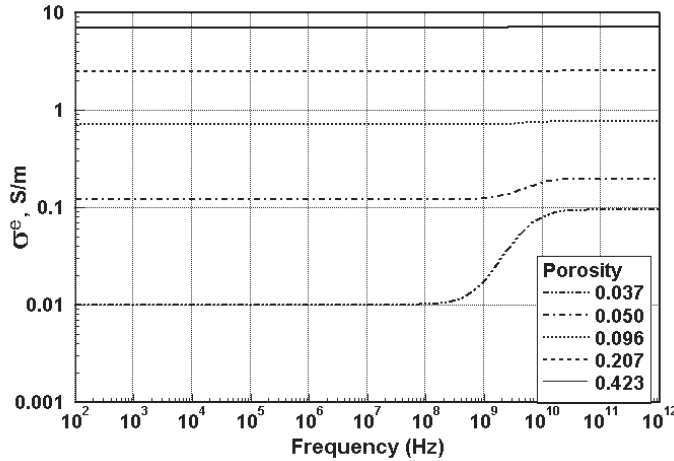

Figure 7. Dispersion of effective conductivity for the Q_8-structure as in Fig. 1(d). The component data are those in Fig. 2.
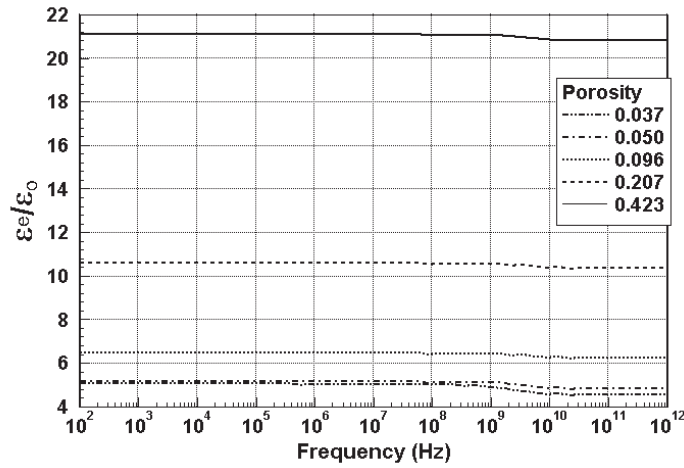
Figure 8. Dispersion of relative effective dielectric permittivity for the Q_8-structure as in Fig. 1(d). The component data are those in Fig. 2.
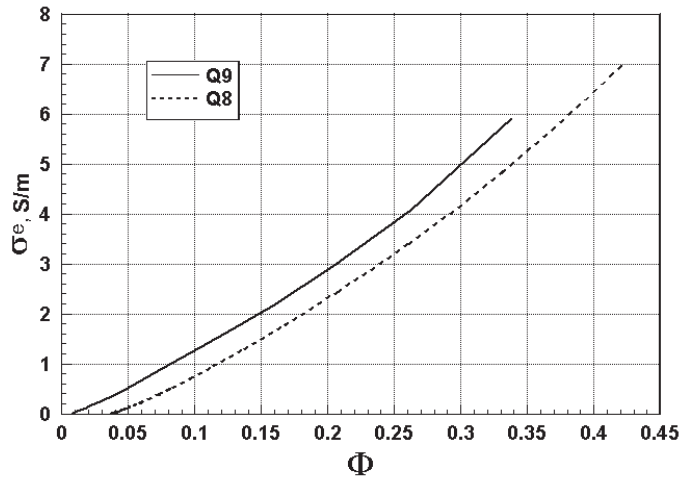

Figure 9. Effective conductivity versus porosity for DC frequencies via homogenization approach. The component data are those in Fig. 2.

average electric conductivity σ_f of the pore fluid is $25\,\mathrm{S/m}$. Commonly, the characteristic frequency f of geophysical logging devices does not exceed $2 \cdot 10^6\,\mathrm{Hz}$. In this case conditions (A6) are satisfied with

$\delta \leq 10^{-2}$, and the homogenized Maxwell equations are given by (13). It follows from Fig. 7 and Fig. 8 that the dispersion effect occurs for frequencies which are much higher than $2 \cdot 10^6$ Hz.

4. ARCHIE-LIKE LAWS

The homogenization formulae derived in Section 2 enable us to plot σ^h versus the fluid volume fraction $\Phi \equiv \Phi_f$ for DC frequencies. It easily follows from (10) that the law $\sigma^h(\Phi)$ is an interpolation function: $\sigma_{pj}^h(0) = \sigma_s \delta_{pj}$ and $\sigma_{pj}^h(1) = \sigma_f \delta_{pj}$, where $\delta_{pj} = 1$ if $p = j$ and $\delta_{pj} = 0$ otherwise. It should be noted that the Archie law (1942) $\sigma/\sigma_f = \Phi^m$ is also an interpolation formula if $\sigma_s = 0$; in contrast, the mixing rule (21) does not meet this important requirement.

We perform calculations of $\sigma^h(\Phi)$ for DC frequencies both for Q_8^r and Q_9^r structures (Fig. 9). "Cementation growth" of r results in pore volume decrement, i.e., decrease of Φ. For both configurations, the function $\sigma^h(\Phi)$ vanishes when $\Phi = \Phi_p$, the percolation threshold depending on the configuration. The fact that the Q_9^r-curve is below the Q_8^r-curve can be explained as follows. To be of the same porosity as the Q_9^r-structure rock, the Q_8^r-configuration should be composed of spheres with great enough radius. As a result, the Q_8^r-configuration has narrower minimal pore throats, lower permeability, and lower conductivity than the Q_9^r-configuration rock of the same porosity. Geometrical aspects of pore throats are discussed thoroughly in [2, 38].

If the Archie formula were in agreement with the homogenization curve $\sigma^h(\Phi)$, the derivative $m = \partial \ln(\sigma^h/\sigma_f)/\partial \ln \Phi$ would be constant as a function of Φ. For both Q_8^r and Q_9^r geometries, Fig. 10 and Fig. 11 show that variation of the cementation factor m versus Φ is significant. Similarly, if one substitutes the Archie law by the Archie percolation formula

$$\sigma = a\sigma_f(\Phi - \Phi_p)^m, \quad a = \text{const}, \quad m = \text{const}, \qquad (22)$$

the derivative $m(\phi) = \partial \ln(\sigma^h/\sigma_f)/\partial \ln(\Phi - \Phi_p)$ will fail to be constant also (Fig. 10, Fig. 11) both for Q_8^r and Q_9^r cases though $\partial \ln(\sigma^h/\sigma_f)/\partial \ln(\Phi - \Phi_p)$ is much closer to a constant then the function $\partial \ln(\sigma^h/\sigma_f)/\partial \ln \Phi$. Nevertheless, one may attempt to find the best Archie approximation for $\sigma^h(\Phi)$ among functions (22). To define suitable a and m, we minimize the functional

$$J(a, m) \equiv \int_{\Phi_2}^{\Phi_1} \left\{ \ln \sigma^h(\Phi) - \ln \left[a\sigma_f(\Phi - \Phi_p)^m \right] \right\}^2 d\Phi.$$
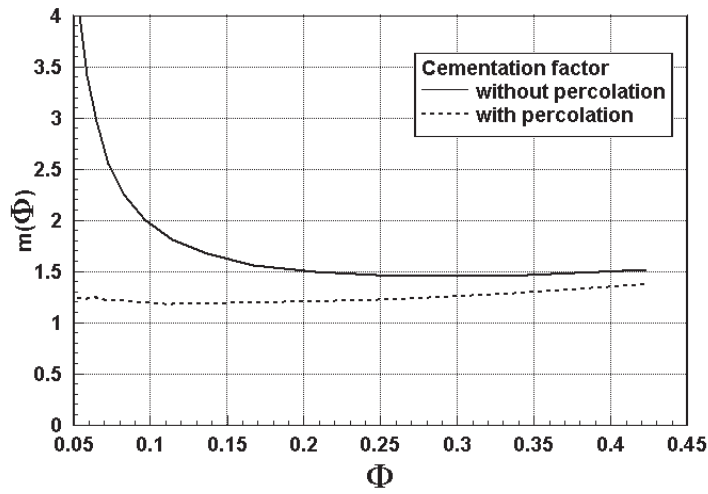
Figure 10. Cementation factor versus porosity via homogenization approach for the Q_8 structure as in Fig. 1(d). The component data are those in Fig. 2.
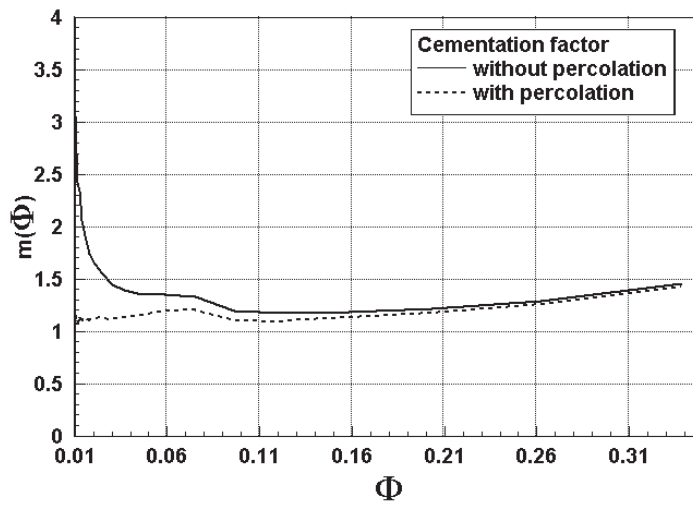

Figure 11. Cementation factor versus porosity via homogenization approach for the Q_9 structure as in Fig. 1(f). The component data are those in Fig. 2.

Here, Φ_1 is the maximal porosity; $\Phi_1 = 0.476$ and $\Phi_1 = 0.320$ for the Q_8^r and Q_9^r geometries respectively. We take $\Phi_2 = 0.13683$ for the Q_8^r-case and $\Phi_2 = 0.09636$ for the Q_9^r-case as the minimal porosities to meet available data on Archie-like statistical formulae. Calculations reveal that $a = 1.20332$ and $m = 1.46$ for the Q_8^r-case, and $a = 1.1914$ and $m = 1.42$ for the Q_9^r-case.

Let us comment on tortuosity of the Q_9^r-structure. If the spheres overlapping is small the fluid channels are not tortuous enough since they contain thin pure fluid tubes of infinite length. Such fluid tubes disappear if the overlapping is strong; it occurs when the sphere radius r becomes greater than $r_t = 1/2$, with the corresponding porosity Φ_t. One can observe in Fig. 11 that $m(\Phi)$ attains a local maximum when $\Phi = \Phi_t$.

5. CONCLUSIONS

We developed a mixing law theory for effective dielectric permittivity and effective electric conductivity by two-scale homogenization of the Maxwell equations. We have proved that the homogenized Maxwell equations are different for low and high frequencies. The approach is well justified for rocks with periodical structure, and it gives rise to a numerical algorithm which works well both for DC and AC frequencies. The code was tested successfully for the cubic array of nonintersecting spheres embedded in a matrix by means of comparing effective parameters obtained by the two-scale homogenization presented here and those computed by traditional mixture formulae such as the Hanai-Bruggeman formula.

As for real rock structures, calculations were performed for two rock models, with solid grains being intersecting spheres of the same radius. The first periodicity cell is formed of eight spheres centered at the unit cube vertices. The second cell of periodicity has one more sphere in the center of the cube. The Maxwell-Wagner dispersion effect is revealed to take place at rather high frequencies. Nevertheless, a shift of the Maxwell-Wagner dispersion phenomena into the low frequency domain is possible when the rock cell is filled with plate grains. This suggestion is due to the analytic dispersion curve which we found for the cell with layered structure.

The homogenization method enables us to comment on the Archie formula. New inconsistencies of the Archie law were discovered. Particularly, we made it clear that porosity was not the only geometrical factor of importance in calculating effective conductivity (Fig. 9); the percolation threshold should be taken into account as well, and the cementation factor m depends

significantly on the interval where porosity varies. Interestingly, according to our calculations, the value of m is close to 1.5 for the best Archie percolation approximation (22) of the homogenization conductivity/porosity curve.

Though in the present paper we considered rocks with simple geometrical structures, the method can be applied to rocks with complex structures as well, in contrast to other mixing rules. Moreover, the method allows us to take into account polarization of solid and fluid components.

ACKNOWLEDGMENT

APPENDIX A.

Here, we use the Gauss system of units. It enables us to correctly check different terms of the Maxwell equations against the small parameter δ defined in Section 2.1. To make presentation self-consistant, we develop a two-scale asymptotic analysis of the Maxwell equations making some important repetitions of the calculations performed in Section 2.1. Given density of the time-harmonic source current $J_s = e^{-i\omega t}\mathbf{f}(x)$, the incident electric and magnetic fields $E := e^{-i\omega t}\mathbf{E}(x)$, $D := e^{-i\omega t}\mathbf{D}(x)$, $H := e^{-i\omega t}\mathbf{H}(x)$, $B := e^{-i\omega t}\mathbf{B}(x)$, $J := e^{-i\omega t}\mathbf{J}(x)$ solve the Maxwell equations

$$-\frac{i\omega}{c}\mathbf{D} = \text{curl}\mathbf{H} - \frac{4\pi}{c}\mathbf{J} - \frac{4\pi}{c}\mathbf{f}, \quad \frac{i\omega}{c}\mathbf{B} = \text{curl}\mathbf{E}, \quad \text{(A1)}$$

with the material laws

$$\mathbf{D} = \varepsilon(x)\mathbf{E}, \quad \mathbf{B} = \mu(x)\mathbf{H}, \quad \mathbf{J} = \sigma(x)\mathbf{E}. \quad \text{(A2)}$$

We exclude the magnetic fields to switch to the Helmholtz-like equation

$$\text{curl}\left(\frac{1}{\mu}\text{curl}\mathbf{E}\right) = \kappa^2\mathbf{E} + \frac{i4\pi\omega}{c^2}\mathbf{f}, \quad \kappa^2 = \frac{\omega^2\varepsilon + i4\pi\sigma\omega}{c^2}. \quad \text{(A3)}$$

With $\hat{\mathbf{E}}$ standing for the reference value of $\mathbf{E}$, we introduce the dimensionless variables $x_i' = x_i/L$ and

$$\mathbf{E}' = \frac{\mathbf{E}}{\hat{E}}, \, \mathbf{D}' = \frac{\mathbf{D}}{\hat{E}}, \, \mathbf{H}' = \frac{\mathbf{H}}{\hat{H}}, \, \mathbf{B}' = \frac{\mathbf{B}}{\hat{H}}, \, \mathbf{J}' = \frac{\mathbf{J}}{\hat{J}}, \, \mathbf{f}' = \frac{\mathbf{f}}{\hat{J}}, \, \omega' = \frac{\omega}{\hat{\omega}}, \, \sigma' = \frac{\sigma}{\hat{\sigma}}.$$

Let $\hat{\varepsilon}$ and $\hat{\mu}$ be reference values of ε and μ, $\varepsilon = \hat{\varepsilon}\varepsilon'$, $\mu = \hat{\mu}\mu'$. We chose $\hat{J} = \hat{\sigma}\hat{E}$, then, in the dimensionless variables, Eq. (A3) becomes

$$\mathrm{curl}'\left(\frac{1}{\mu'}\mathrm{curl}'\mathbf{E}'\right) - \kappa'^2\mathbf{E}' = ia_1 4\pi\omega'\mathbf{f}', \qquad (A4)$$

where

$$\kappa'^2 = \omega'^2\varepsilon'\frac{L^2}{l_w^2} + i4\pi\sigma'\omega'\frac{L^2}{l_s^2}, \quad a_1 = \frac{L^2}{l_s^2}, \quad l_w = \frac{c}{\hat{\omega}\sqrt{\hat{\mu}\hat{\varepsilon}}}, \quad l_s = \frac{c}{\sqrt{\hat{\omega}\hat{\sigma}\hat{\mu}}};$$

here, l_w is the wave length and l_s is the skin layer length.

We perform asymptotic analysis of Eq. (A4), assuming that δ is a small parameter. We apply the two-scale homogenization approach [13] and use the dimensionless micro-variables

$$y_j = \frac{x_j'}{\delta}, \quad y \in Y = \{0 < y_j < r_j\}.$$

Here Y is the dimensionless periodicity cell; it consists of solid and fluid parts, $Y = Y_s \cup Y_f$:

$$\varepsilon'(y), \mu'(y), \sigma'(y) = \begin{cases} \varepsilon_s', \mu_s', \sigma_s', & \text{if } y \in Y_s, \\ \varepsilon_f', \mu_f', \sigma_f', & \text{if } y \in Y_f. \end{cases} \qquad (A5)$$

The exact meaning of the assumption on the periodic rock structure is that the coefficients ε', σ', and μ' in Eq. (A4) are periodic step functions

$$\varepsilon'\left(\frac{x'}{\delta}\right), \quad \mu'\left(\frac{x'}{\delta}\right), \quad \sigma'\left(\frac{x'}{\delta}\right),$$

with the period δr_j in each variable x_j'. First, we consider the case of low angular frequencies $\hat{\omega}$, i.e., we assume that the skin layer length and wave length are greater than the cell size:

$$\frac{l_j}{l_s} = \alpha_s^j\delta, \quad \frac{l_j}{l_w} = \alpha_w^j\delta. \qquad (A6)$$

For simplicity, we assume that the ratios α_s^j/r_j and α_w^j/r_j are independent of index j.

Under the hypothesis (A6), we have

$$\frac{L}{l_s} = \frac{\alpha_s^1}{r_1} \equiv \alpha_s, \quad \frac{L}{l_w} = \frac{\alpha_w^1}{r_1} \equiv \alpha_w.$$

Hence, κ'^2 does not depend on δ and

$$\kappa'^2 = \alpha_w^2 \omega'^2 \varepsilon' + i4\pi\alpha_s^2 \omega'\sigma'. \tag{A7}$$

For simplicity, we drop the prime superscript in what follows. We denote

$$\frac{\mathrm{curl}\mathbf{E}(x)}{\mu(x/\delta)} = \mathbf{M}(x), \quad \kappa^2(x/\delta)\mathbf{E}(x) = \mathbf{N}(x). \tag{A8}$$

Thus,

$$\mathrm{curl}\mathbf{M} - \mathbf{N} = i4\pi\omega\alpha_s^2\mathbf{f}. \tag{A9}$$

We look for a solution of (A8) and (A9) in the form

$$\mathbf{E}(x) = \{\mathbf{E}^0(x, y) + \delta\mathbf{E}^1(x, y) + o(\delta)\}|_{y=x/\delta}, \tag{A10}$$

$$\mathbf{M}(x) = \{\mathbf{M}^0(x, y) + \delta\mathbf{M}^1(x, y) + o(\delta)\}|_{y=x/\delta}, \tag{A11}$$

$$\mathbf{N}(x) = \{\mathbf{N}^0(x, y) + \delta\mathbf{N}^1(x, y) + o(\delta)\}|_{y=x/\delta}, \tag{A12}$$

where all the functions are periodic in variable y_j with period r_j. It should be noted that variables x, y, and δ in these formulae are treated as independent and

$$\mathrm{curl}\mathbf{E}^k(x, x/\delta) = \left\{ \mathrm{curl}_x\,\mathbf{E}^k(x, y) + \frac{1}{\delta}\mathrm{curl}_y\,\mathbf{E}^k(x, y) \right\}|_{y=x/\delta}.$$

Putting the representation formulae (A10)–(A12) in (A8) and (A9), one can write each of these equalities in the form

$$\sum_{-1}^{0} \delta^k(\cdots)_k + O(\delta) = 0.$$

To find all the coefficients in the series (A10)–(A12), one should solve all the equations $(\cdots)_k = 0$, $k = -1, 0$. Particularly, one would find from (A8) that

$$\mathrm{curl}_y\mathbf{E}^0 = 0, \quad \mathbf{M}^0 = \frac{1}{\mu(y)}\left(\mathrm{curl}_x\mathbf{E}^0 + \mathrm{curl}_y\mathbf{E}^1\right),$$

$$\mathbf{N}^0 = \kappa^2(y)\mathbf{E}^0. \tag{A13}$$

Let

$$\tilde{\mathbf{E}}(x) = \frac{1}{|Y|}\int_Y \mathbf{E}^0(x, y)dy$$

stand for the average value of $\mathbf{E}^0(x, y)$ over the cell Y; the functions $\tilde{\mathbf{M}}(x)$ and $\tilde{\mathbf{N}}(x)$ are defined similarly. It follows from $(A13)_1$ that there is a periodic (in the variable y) function $\varphi^0(x, y)$ such that

$$\mathbf{E}^0(x, y) = \tilde{\mathbf{E}}(x) + \nabla_y \varphi^0(x, y). \qquad (A14)$$

On the other hand, because of (A9), we have

$$\mathrm{div}(\mathbf{N} + i4\pi\alpha_s^2\omega\mathbf{f}) = 0. \qquad (A15)$$

Making use of the representation formula (A12) and the formula

$$\mathrm{div}\mathbf{N}^0(x, x/\delta) = \left\{ \mathrm{div}_x \mathbf{N}^0(x, y) + \frac{1}{\delta}\mathrm{div}_y \mathbf{N}^0(x,y) \right\}|_{y=x/\delta}, \qquad (A16)$$

we conclude from (A15) that $\mathrm{div}_y\mathbf{N}^0 = 0$. Now, it follows from $(A13)_3$ and (A14) that the function $\varphi^0(x, y)$ is periodic in y and solves the equation

$$\mathrm{div}_y\left\{ \kappa^2(y)\left(\tilde{\mathbf{E}} + \nabla_y\varphi^0 \right) \right\} = 0. \qquad (A17)$$

We look for $\varphi^0(x, y)$ by the method of separation of variables in the form

$$\varphi^0(x, y) = \tilde{E}_j(x)w_\varepsilon^j(y),$$

where w_ε^j is periodic in y. Putting this sum into (A17), one can uniquely define functions $w_\varepsilon^j(y)$ as periodic solutions to the cell boundary-value problems

$$\frac{\partial}{\partial y_p}\left\{ \kappa^2(y)\frac{\partial}{\partial y_p}\left(y_j + w_\varepsilon^j(y) \right) \right\} = 0, \quad \int_Y w_\varepsilon^j(y)dy = 0. \qquad (A18)$$

Function $\kappa^2(y)$ is discontinuous across the surface Γ separating solid and fluid domains of Y; therefore Eq. $(A18)_1$ holds in the distribution sense. Particularly, Eq. $(A18)_1$ suggests that the following no-jump condition is true at Γ:

$$\left[\kappa^2\mathbf{n} \cdot \nabla(y_j + w_\varepsilon^j) \right] = 0,$$

where the brackets $[f]$ stand for a jump of a discontinuous function f across Γ and $\mathbf{n}$ is the unit normal vector to Γ. Given the micro-functions $w_\varepsilon^j(y)$, we find from $(A13)_3$ that

$$\tilde{\mathbf{N}} = \frac{1}{|Y|}\int_Y \kappa^2(y)\mathbf{E}^0(x,y)dy \quad \text{or} \quad \tilde{N}_p(x) = (\kappa^2)_{pj}^h\tilde{E}_j(x), \qquad (A19)$$

where

$$(\kappa^2)^h_{pj} = \frac{1}{|Y|} \int_Y \kappa^2(y) \frac{\partial}{\partial y_p} \left(y_j + w^j_\varepsilon(y) \right) dy. \qquad (A20)$$

We use the superscript h both to emphasize that the constant matrix (A20) is a material parameter of a homogenized medium and to distinguish this constant matrix from the step function (A7).

We return to (A9) and find, because of (A11) and (A12), that

$$\mathrm{curl}_y \mathbf{M}^0 = 0. \qquad (A21)$$

On the other hand, we obtain from (A16) and the equality $\mathrm{div}(\mu(x/\delta)\mathbf{M}) = 0$ that

$$\mathrm{div}_y \left(\mu(y)\mathbf{M}^0 \right) = 0. \qquad (A22)$$

By the same arguments as in the case of the function $\mathbf{E}^0$, we derive from (A21) and (A22) that

$$\mathbf{M}^0(x,\, y) = \tilde{\mathbf{M}}(x) + \tilde{M}_j(x)\nabla_y w^j_\mu(y), \qquad (A23)$$

where the periodic functions $w^j_\mu(y)$ solve the cell problems

$$\frac{\partial}{\partial y_p} \left\{ \mu(y) \frac{\partial}{\partial y_p} \left(y_j + w^j_\mu(y) \right) \right\} = 0, \quad \int_Y w^j_\mu(y) dy = 0. \qquad (A24)$$

We multiply $(A13)_2$ by $\mu(y)$ and integrate over the cell Y taking into account that $\int_Y \mathrm{curl}_y \mathbf{E}^1 \, dy = 0$ by periodicity. As a result, we obtain

$$\mathrm{curl}_x \tilde{\mathbf{E}} = \frac{1}{|Y|} \int_Y \mu(y)\mathbf{M}^0(x,y)dy$$

or

$$\left(\mathrm{curl}_x \tilde{\mathbf{E}} \right)_p = \mu^h_{pj}\tilde{M}_j(x), \qquad (A25)$$

where

$$\mu^h_{pj} = \frac{1}{|Y|} \int_Y \mu(y) \frac{\partial}{\partial y_p} \left(y_j + w^j_\mu(y) \right) dy. \qquad (A26)$$

It follows from (A9) that

$$\mathrm{curl}_x \mathbf{M}^0 + \mathrm{curl}_y \mathbf{M}^1 - \mathbf{N}^0 = i4\pi\omega a_1 \mathbf{f}.$$

We integrate it over the cell Y to arrive at the equality

$$\mathrm{curl}_x \tilde{\mathbf{M}} - \tilde{\mathbf{N}} = i4\pi\omega\alpha_s^2 \mathbf{f}. \tag{A27}$$

Again, we have used that $\int_Y \mathrm{curl}_y \mathbf{M}^1 \, dy = 0$ by periodicity. Thus, putting together equalities (A27), (A19), and (A25), we obtain the macro-equation

$$\mathrm{curl}_x \left\{ \left(\mu^h\right)^{-1} \cdot \mathrm{curl}_x \tilde{\mathbf{E}} \right\} - (\kappa^2)^h \cdot \tilde{\mathbf{E}} = i4\pi\omega\alpha_s^2 \mathbf{f}, \tag{A28}$$

where $\left(\mu^h\right)^{-1}$ is the inverse of matrix μ^h.

Let us consider the case of high frequencies:

$$\frac{l_j}{l_s} = \frac{\alpha_s^j}{\delta^m}, \quad \frac{l_j}{l_w} = \frac{\alpha_w^j}{\delta^m}, \quad m \geq 0, \tag{A29}$$

where the ratios α_s^j/r_j and α_w^j/r_j are independent of index j. With this hypothesis at hand, we have

$$\frac{L}{l_s} = \frac{\alpha_s^1}{\delta^q r_1} \equiv \frac{\alpha_s}{\delta^q}, \quad \frac{L}{l_w} = \frac{\alpha_w^1}{\delta^q r_1} \equiv \frac{\alpha_w}{\delta^q}, \quad q \geq 1.$$

Hence, κ'^2 depends on δ and

$$\kappa'^2 = \frac{(k_1')^2}{\delta^{2q}}, \quad (k_1')^2 \equiv \alpha_w^2 \omega'^2 \varepsilon' + i4\pi\alpha_s^2 \omega' \sigma'. \tag{A30}$$

Equation (A9) becomes

$$\mathrm{curl}' \left(\frac{1}{\mu'} \mathrm{curl}' \mathbf{E}' \right) - \frac{(k_1')^2}{\delta^{2q}} \mathbf{E}' = \frac{i4\pi\omega'\alpha_s^2}{\delta^{2q}} \mathbf{f}'. \tag{A31}$$

We perform asymptotical analysis of these equations dropping the prime superscript. Denoting

$$\frac{\mathrm{curl}\mathbf{E}(x)}{\mu(x/\delta)} = \mathbf{M}(x), \quad k_1^2(x/\delta)\mathbf{E}(x) = \mathbf{N}(x), \tag{A32}$$

we write out Eq. (A31) as

$$\mathrm{curl}\mathbf{M} - \frac{1}{\delta^{2q}}\mathbf{N} = \frac{i4\pi\omega\alpha_s^2}{\delta^{2q}}\mathbf{f}. \tag{A33}$$

We look for a solution of (A33) in the form (A10)–(A12). By the above arguments, we obtain

$$\mathrm{curl}_y \mathbf{E}^0 = 0, \quad \mathbf{N}^0 = k_1^2(y)\mathbf{E}^0, \quad \mathrm{div}_y \mathbf{N}^0 = 0. \tag{A34}$$

Hence,

$$\mathbf{E}^0(x,\,y) = \tilde{\mathbf{E}}(x) + \tilde{E}_j(x)\nabla_y w_\varepsilon^j(y), \qquad (A35)$$

where the periodic functions $w_\varepsilon^j(y)$ solve the cell problems (A18) with κ^2 substituted by k_1^2. It follows from $(A34)_2$ that

$$\tilde{N}_p(x) = (k_1^2)_{pj}^h \tilde{E}_j(x), \qquad (A36)$$

where the matrix $(k_1^2)_{pj}^h$ is given by the right-hand side of formula (A20) with $\kappa^2(y)$ substituted by $k_1^2(y)$.

It follows from (A33) that

$$-\mathbf{N}^0 = i4\pi\omega\alpha_s^2\mathbf{f}.$$

Let us integrate this equation over the cell Y, making use of the equality $(A34)_2$. As a result, we obtain the macro-equation in the high frequency region:

$$-(k_1^2)^h \cdot \tilde{\mathbf{E}} = i4\pi\omega\alpha_s^2\mathbf{f}. \qquad (A37)$$

Returning to the dimensional variables, we conclude that, in the SI unit system, the effective parameters are given by the representation mixing formulae (9)–(11), and the macro-equations (A28) and (A37) become (13) and (14) respectively.

REFERENCES

1. Sihvola, A., *Electromagnetic Mixing Formulae and Applications*, The Institution of Electric Engineers, London, 1999.
2. Herrick, D. C. and W. D. Kennedy, "Electrical efficiency: A pore geometric theory for interpretation of the electrical properties of reservoir rocks," *Geophysics*, Vol. 59, No. 6, 918–927, 1994.
3. Allaire, G., "Homogenization and two-scale convergence," *SIAM J. Math. Anal.*, Vol. 23, No. 6, 1482–1518, 1992.
4. Bakhvalov, N. and G. Panasenko, *Homogenization: Averaging Processes in Periodic Media*, Kluwer, Dordrecht, 1989.
5. Beliaev, A. Y., *Homogenization in the Problems of Groundwater Flows*, Nauka, Moscow, 2004.
6. Bensoussan, A., J.-L. Lions, and G. Papanicolau,, *Asymptotic Analysis for Periodic Structures*, North-holland, Amsterdam, 1978.
7. Coiranescu, D. and P. Donato, *An Introduction to Homogenization*, Number 17 in Oxford Lecture Series in Mathematics and Its Applications, Oxford University Press, 1999.

8. Dal Maso, G., *An Introduction to Gamma-Convergence*, Boston, 1993.

9. De Giorgi, E., "Sulla convergenza di alcune successioni d'integrali del tipo dell'area," *Rend. Mat.*, Vol. 8, No. 6, 277–294, 1975.

10. Murat, F., "Compacité par compensation, Partie I," *Ann. Scuola Norm. Sup. Pisa, Cl. Sci. Fis. Mat.* Vol. 5, 489–507, 1978.

11. Murat, F., "Compacité par compensation, Partie II," *Proc. Intern. Meeting on Recent Methods in Nonlinear Analysis*, De Giorgi (ed.), Magenes, Mosco, Pitagora, Bologna, 245–256, 1979.

12. Nguetseng, G., "A general convergence result for a functional related to the theory of homogenization," *SIAM J. Math. Anal.*, Vol. 20, No. 3, 608–623, 1989.

13. Sanchez-Palencia, E., *Non-homogeneous Media and Vibration Theory*, Lecture notes in Phys. Springer, New York, 1980.

14. Spagnolo, S., "Sul limite delle soluzioni di problemi di Cauchy relativi all'equazione del calore," *Ann. Scuola Norm. Sup. Pisa, Cl. Sci. Fis. Mat.*, Vol. 21, No. 3, 657–699, 1967.

15. Tartar, L., "Problèmes d'homogénéisation dans les équations aux dérivées partielles," *H-convergence*, F. Murat (ed.), Cours Peccot Collège de France, *Séminare d'Analyse Fonctionnelle et Numérique*, 1977/78, Université d'Alger, 1978.

16. Zhikov, V. V., Kozlov, S. M., Oleinik, O. A., *Homogenization of Differential Operators and Integral Functionals*, Springer-Verlag, Berlin etc. 1994.

17. Bakhvalov, N. S., "Homogenized characteristics of bodies with periodic structures," *Doklady Mathematics of USSR*, Vol. 218, No. 5, 1046–1048, 1974.

18. Caillerie, D., Lévy, T., "Application de l'homogénéisation au compartement électromagnétic d'un mélange isolant-conducteur," *C. R. Acad. Sc. Paris*, Vol. 296, Ser. II, 1035–1038, 1983.

19. Engström, C. and D. Sjöberg, "On two numerical methods for homogenization of Maxwell's equations," *Journal of Electromagnetic Waves and Applications*, Vol. 21, No. 13, 1845–1856, 2007.

20. Kristensson, G., "Homogenization of the Maxwell equations in an anisotropic material," Technical Report LUTEDX/(TEAT-7124)/1-12/(2001), Department of Electroscience, Lund Institute of Technology, Sweeden, 2001.

21. Markowich, P. A. and F. Poupaud, "The Maxwell equation in a periodic medium: Homogenization of the energy density," *Ann. Sc. Norm. Sup. Pisa Cl. Sci.*, Vol. 23, No. 4, 301–324, 1996.

22. Sjöberg, D., "Homogenizatopn of dispersive material parameters

for Maxwell's equations using a singular value decomposition," Technical Report LUTEDX/(TEAT-7124)/1-24/(2004), Department of Electroscience, Lund Institute of Technology, Sweeden, 2004.

23. Sjöberg, D., C. Engström, G. Kristensson, D. J. N. Wall, and N. Wellander, "A floquet-bloch decomposition of Maxwell's equations, applied to homogenization," Technical Report LUTEDX/(TEAT-7119)/1-27/(2003), Department of Electroscience, Lund Institute of Technology, Sweeden, 2003.

24. Wellander, N., "Homogenization of the Maxwell equations: Case I. Linear theory," *Appl. Math.*, Vol. 46, No. 2, 29–51, 2001.

25. Wellander, N., "Homogenization of the Maxwell equations: Case II. Nonlinear conductivity," *Appl. Math.*, Vol. 47, No. 3, 255–283, 2002.

26. Banks, H. T., V .A. Bokil, D. Ciroanescu, N. L. Gibson, G. Griso, and B. Miara, "Homogenization of periodically varying coefficients in electromagnetic materials," *J. Sci. Comput.*, Vol. 28, No. 2–3, 191–221, 2006.

27. Bosavit, A., G. Griso, and B. Miara, "Modélisation de structures électromanetiques périodiques: Matériaux bianisotropiques avec mémoire," *C.R. Acad. Sci. Paris*, Ser. I, Vol. 338, 97–102, 2004.

28. Huang, K. and X. Yang, "A method for calculating the effective permittivity of a mixture solution during a chemical reaction by experimental results," *Progress In Electromagnetics Research Letters*, Vol. 5, 99–107, 2008.

29. Artola, M., "Homogenization and electromagnetic wave propagation in composite media with high conductivity inclusions," *Proceedings of the Second Workshop on Composite Media and Homogenization Theory*, D. Maso and G. Dell'Anttotnio (eds.), Singapore, World Scientifis Publisher, 2005.

30. Kristensson, G., "Homogenization of corrugated interfaces in electromagnetics," *Progress In Electromagnetics Reserach*, PIER 55, 1–31, 2005.

31. Ouchetto, O., S. Zouhdi, A. Bossavit, G. Griso, and B. Miara, "Modeling of 3D periodic multiphase composites by homogenization," *Transactions on Microwave Theory and Techniques*, Vol. 54, No. 6, Part 2, 2615–2619, 2006.

32. Wellander, N. and G. Kristensson, "Homogenization of the Maxwell equations at fixed frequency," *SIAM J. Appl. Math.*, Vol. 64, No. 1, 170–195, 2003.

33. Garrouch, A. A. and M. M. Sharma, "The influence of clay con-

tents, salinity, stress, and wettability on the dielectric properties of brine-saturated rocks: 10 Hz to 10 MHz," *Geophysics*, Vol. 59, No. 6, 909–917, 1994.

34. El Feddi, M., Z. Ren, A. Razek, and A. Bossavit, "Homogenization technique for Maxwell equations in periodic structures," *IEEE Transactions on Magnetics*, Vol. 33, No. 2, 1382–1385, 1997.

35. Hashin, Z. and S. Shtrikman, "A variational approach to the theory of effective magnetic permeability of multiphase materials," *J. Appl. Phys.*, Vol. 33, 3125–3131, 1962.

36. Sihvola, A., "Effective permittivity of mixtures: Numerical validation by the FDTD method," *IEEE Transactions on Geosciences and Remote Sensing*, Vol. 38, No. 3, 1303–1308, 2000.

37. Vinogradov, A. P., *Electrodynamics of Composite Materials*, Editorial, URSS, Moscow, 2001.

38. Roberts, J. N. and L. M. Schwartz, "Grain consolidation and electrical conductivity in porous media," *Physical Review B*, Vol. 31, No. 9, 5990–5997, 1985.

39. Jackson, J. D., *Classical Electrodynamics*, 2nd edition, John Wiley & Son, New York, 1975.

40. Maxwell, J. C., *Treatise on Electricity and Magnetism*, Vol. 21, Clarendon Press, Oxford, 1881.

41. Wagner, K. W., *Aroh Elektrotech*, No. 9, 371–392, 1914.

42. Brawn, W. F. Jr., *Dielectrics*, Handbuch der Physik. Herausgegeben von S. Figgre, Band XVII, S. 1, Springer-Verlag, Berlin-Gettingen-Heidelberg, 1956.

43. Dykhne, A. M., "Conductivity of a two-dimensional two-phase system," *Journal of Experimental and Theoretical Physics*, Vol. 59, No. 7, 110–115, 1970.

44. Talalov, A. D. and D. S. Daev, "On a structure mechanism undelying dispersion of electrical properties of heterogeneous rocks," *Izvesiya, Physics of the Solid Earth*, Vol. 8, 56–66, 1996.

45. Zuzovsky, M. and H. Brenner, "Effective conductivities of composite materials composed of cubic arrangements of spherical particles embedded in an isotropic matrix," *J. Appl Math. Phys.*, Vol. 28, 979–992, 1977.